Mixed bioconvection stagnation point flow towards a vertical plate in alumina-copper/water

Nurul Amira Zainal
Department of Mathematical Sciences, Faculty of Science and Technology, Universiti Kebangsaan Malaysia, Bangi, Malaysia and Fakulti Teknologi Kejuruteraan Mekanikal dan Pembuatan, Universiti Teknikal Malaysia Melaka, Durian Tunggal, Malaysia

Roslinda Nazar
Department of Mathematical Sciences, Faculty of Science and Technology, Universiti Kebangsaan Malaysia, Bangi, Malaysia

Kohilavani Naganthran
Center for Data Analytics Consultancy and Services, Universiti, Kuala Lumpur, Malaysia and Institute of Mathematical Sciences, Universiti, Kuala Lumpur, Malaysia, and

Ioan Pop
Department of Mathematics, Babes-Bolyai University, Cluj-Napoca, Romania

Received 22 October 2021
Revised 14 January 2022
9 February 2022
Accepted 9 February 2022

Abstract

Purpose – According to the previous research, bioconvection has been recognized as an important mechanism in current engineering and environmental systems. For example, researchers exploit this mechanism in modern green bioengineering to develop environmentally friendly fuels, fuel cells and photosynthetic microorganisms. This study aims to analyse how this type of convection affects the flow behaviour and heat transfer performance of mixed convection stagnation point flow in alumina-copper/water hybrid nanofluid. Also, the impact of a modified magnetic field on the boundary layer flow is considered.

Design/methodology/approach – By applying appropriate transformations, the multivariable differential equations are transformed into a specific sort of ordinary differential equations. Using the bvp4c procedure, the adjusted mathematical model is revealed. Once sufficient assumptions are provided, multiple solutions are able to be produced.

Findings – The skin friction coefficient is declined when the nanoparticle concentration is increased in the opposing flow. In contrast, the inclusion of aligned angles displays an upward trend in heat transfer performance. The presence of several solutions is established, which simply leads to a stability analysis, hence verifies the viability of the initial solution.

Originality/value – The current findings are unique and novel for the investigation of mixed bioconvection flow towards a vertical flat plate in a base fluid with the presence of hybrid nanoparticles.

Keywords Hybrid nanofluid, Stagnation point flow, Magnetohydrodynamics, Mixed bioconvection

Paper type Research paper

International Journal of Numerical Methods for Heat & Fluid Flow
Vol. 32 No. 11, 2022
pp. 3413-3438

0961-5539
DOI 10.1108/HFF-10-2021-0693

This project is funded by GUP-2019–034 from UKM, Malaysia.

Nomenclature

Roman letters

a,b = constant (–);
c = concentration of the fluid (M/kg);
C_f = skin friction coefficient (–);
C_p = specific heat at constant pressure (Jkg^{-1}/K^{-1});
C_w, C_∞ = far and ambient concentration (–);
D_B = Brownian diffusion coefficient for concentration (m^2s^{-1});
D_n = Brownian diffusion coefficient for motile microorganism (m^2s^{-1});
$f(\eta)$ = dimensionless stream function (–);
g = gravity acceleration (ms^{-2});
(ρC_p) = heat capacitance of the fluid ($JK^{-1}m^{-3}$);
k = thermal conductivity of the fluid (Wm^{-1}/K^{-1});
L = characteristic length of the sheet surface (–);
Le = conventional Lewis number (–);
Lb = bioconvection Lewis number (–);
M = magnetic parameter (–);
N = number of density microorganism (–);
N_w, N_∞ = far and ambient uniform concentration of microorganisms (–);
Nn_x = local motile concentration microorganism number;
Nu_x = local Nusselt number (–);
Pe = Peclet number (–);
Pr = Prandtl number (–);
Re_x = local Reynolds number (–);
Sh_x = local Sherwood number (–);
t = time (s);
T = temperature of fluid (K);
T_0 = temperature of surface (K);
T_∞ = ambient temperature (K);
u = velocity component in x-direction (ms^{-1});
v = velocity component in y-direction (ms^{-1});
u_e = velocity of the ambient (inviscid) fluid in the x-axis (ms^{-1}); and
w_c = velocity of the cell swimming (ms^{-1}).

Greek symbols

σ = electrical conductivity (–);
β = coefficient of thermal expansion (–);
ε = eigenvalue (–);
ε_1 = smallest eigenvalue (–);
ϕ_1, ϕ_2 = volume fractions of nanoparticle for Al_2O_3 and Cu (–);
γ = acute angle (–);
λ = mixed convection parameter (–);
η = similarity variable (–);
θ = dimensionless temperature (–);
μ = dynamic viscosity of the fluid ($kgm^{-1}s^{-1}$);
v = kinematic viscosity of the fluid (m^2s^{-1});
ρ = density of the fluid (kgm^{-3});
τ = dimensionless time variable (–); and
Λ = buoyancy ratio parameter (–).

Subscripts
f = base fluid (–);
nf = nanofluid (–);
hnf = hybrid nanofluid (–);
$s1$ = solid component for Al_2O_3 (alumina) (–); and
$s2$ = solid component for Cu (copper) (–).

Superscript
$'$ = differentiation with respect to η (–).

1. Introduction

Human society dwells in progressive technology where heat transfer is critical in a variety of industries, including power generation, electronic devices and others. This ongoing improvement involves improved system operation and performance, as well as the pursuit of a new cooling technology revolution. In this scenario, the thermal management of such equipment is remarkable, demanding the invention of an efficient heat transfer medium by researchers. Today, to fulfill the requirement for better heat-conducting properties in traditional fluids, the hybrid nanofluid is invented. This new nanofluid composition aims to enhance thermal conductivity significantly. Soon after the innovative discoveries of Choi and Eastman (1995) that gave rise to the brilliant idea of nanofluid, a new generation of fluids has been found and intensively examined. These fluids that are made up of a number of solid components dispersed in a conservative fluid and are known as hybrid nanofluids. According to current experimental and numerical investigations, hybrid nanofluids are operating fluids that have the potential to significantly optimize the thermal efficiency. However, additional research concerning hybrid nanofluid interactions is needed (see Huminic and Huminic (2018)).

The effect of heat conductivity by suspending mono and hybrid nanoparticles was examined by Das (2017) and Hamzah *et al.* (2017). The study reported that in comparison to ordinary nanofluids, the hybrid nanofluid has better thermal conductivity. The most recent research on the use of hybrid nanofluids has been reviewed by Jamil and Ali (2020), Shah and Ali (2019); Khashi'ie *et al.* (2021); and Yang *et al.* (2020). Waini *et al.* (2020) investigated thermal performance towards a permeable moving wedge while taking magnetic parameter execution into consideration in hybrid nanofluid. The influence of magnetohydrodynamics (MHD) stagnation point flow on a permeable moving surface with buoyancy effect is addressed by Hussain *et al.* (2021); Zainal *et al.* (2020a, 2021a); and Jamaludin *et al.* (2020). Some available reviews focused on the nanofluid and hybrid nanofluid considering various effects can be assessed through Uddin *et al.* (2015), Ghalambaz *et al.* (2019); Waini *et al.* (2021a); Zainal *et al.* (2021b); Roşca *et al.* (2021a, 2021b, 2021c); and Khan *et al.* (2021).

The classical stagnation point problem in two-dimensional flow was first introduced by Hiemenz (1911). Since then, countless research has been undertaken in recognising the significance of the stagnation point flow in a number of engineering and commercial activities, such as extrusion and the polymer industry (Rauwendaal, 1985; Fisher, 1976). Proudman and Johnson (1961) and Robins and Howarth (1972) developed the boundary layer study at a two-dimensional rear stagnation point, while Howarth (1973) focused on a three-dimensional flow. In another study, Rostami *et al.* (2018) found a dual solution for mixed convective hybrid nanofluid flow, and it has been claimed that hybrid nanofluid can be recommended for heat transfer analysis to enhance the thermophysical properties of conventional fluid and nanofluid. Nadeem *et al.* (2018) observed the behaviour of three-dimensional stagnation point flow towards a circular cylinder in a hybrid nanofluid. The findings revealed that the heat transfer rate in hybrid nanofluid is higher than the

conventional nanofluid. Ever since, plenty of studies on thermal efficiency in stagnation point flow have been conducted by several scholars, for instance, Anuar and Bachok (2021); Waini *et al.* (2021b); Zainal *et al.* (2020b); Roşca *et al.* (2019, 2021d); and Arani and Aberoumand (2021).

In real-world applications, the magnetic field is crucial in altering the field of flow. The evaluation of MHD is crucial in the industry because of its persistent demand in a variety of industrial fields, such as metallurgical procedures and petroleum production (Hartmann, 1937; Leibovich, 1967; Katagiri, 1969). Hartmann (1937) presented the theory of the laminar conductive liquid in a homogeneous magnetic field. Leibovich (1967) performed an investigation towards the MHD flow at a rear stagnation point to study the use of magnetic fields as a valuable tool in a separation process. Katagiri (1969) demonstrated the MHD boundary layer separation by investigating the problem of unsteady rear stagnation point in the presence of an applied magnetic field. Later, Pavlov (1974) used a uniform transverse magnetic field to facilitate the electrically conducting fluids flow in a boundary layer. Raju *et al.* (2015) analysed the effects of an aligned magnetic field which considered the two-dimensional flow past a stretching surface. As per their observations, increasing the aligned angle intensifies the magnetic field, reduces the profile of velocity and upsurges the heat transfer performance. Sulochana *et al.* (2016) investigated the influence of cross-diffusion and aligned magnetic field over an exponential surface on a nanofluid. Uddin *et al.* (2018) performed a numerical study on MHD slip flow over a radiating plate in nanofluid considering Newtonian heating; meanwhile, Beg *et al.* (2021) analysed the energy conservation performance of biomagnetic needle with Stefan blowing effect in a nanofluid.

Further, Al-Mdallal *et al.* (2020) carried out an analytical analysis to scrutinize the effect of an inclined magnetic field with Marangoni radiative effects over a permeable surface in a different type of hybrid nanofluids. It is worth mentioning that based on the reported results, the titanium dioxide-silicon dioxide/water (TiO_2-SiO_2/H_2O) hybrid nanofluid possesses the highest rate of heat transfer compared to aluminium oxide-silicon dioxide/water (Al_2O_3-SiO_2/H_2O) and aluminium oxide-titanium dioxide/water (Al_2O_3-TiO_2/H_2O). A summary of some boundary layer research that studies the impact of the aligned magnetic field is reviewed by Ashwinkumar *et al.* (2018); Abdul Hakeem *et al.* (2020); and Khan *et al.* (2021).

In advanced engineering and environmental systems, bioconvection has emerged as a prominent mechanism. For example, researchers use this mechanism in modern green bioengineering to create more environmentally friendly fuels, fuel cells and photosynthetic microorganisms (Bees and Croze, 2014; Janicek *et al.*, 2014; Jo *et al.*, 2006). Theoretically, the upswimming microorganisms generate an unstable density stratification, which causes this sort of convection. Wager (1911) conducted a detailed observations on bioconvection in 1911. However, Platt (1961), created the term "bioconvection" after he revisited the work done by Wager (1911). Kuznetsov and Avramenko (2004) were the first to explore the topic of bioconvection in suspension-containing nanoparticles. Their finding proved that as the average number density of small particles increases, the critical Rayleigh number rises, implying that the particles stabilize the suspension. This indicates that the bioconvection emerges in nanofluids when the nanoparticles concentration is small, thus the viscosity of the base fluid is not significantly affected by nanoparticles. According to the study by Anoop *et al.* (2009), as microorganisms can survive in the base fluid, a stable nanoparticle suspension with no agglomeration is possible. In another work, Acharya *et al.* (2016) assessed the influence of MHD bioconvection nanofluid with the presence of gyrotactic microbes and solar radiation numerically. Their study revealed that due to the effects of conventional Lewis number, the density of motile microorganisms had been reported to decrease. Day by day, various researchers have been devoting significant efforts to the bioconvection mechanism in nanofluid flow, for instance, see Zaimi *et al.* (2014), Raees *et al.* (2015); Uddin *et al.* (2016); Zohra *et al.* (2019, 2020); and Bhatti *et al.* (2021).

According to the available literature, an investigation of heat transfers and mixed bioconvection stagnation point flow with modified magnetic field effects in Al_2O_3-Cu/H_2O still lacks throughout the scientific studies. Consequently, the current endeavour aims to develop a numerical computational model of hybrid nanofluid and heat transfer following the work done by Tiwari and Das (2017). In addition, to clarify the defined problems, the current study used the bvp4c approach in the MATLAB software. A stability analysis was carried out as the above procedure efficiently established more than one solution.

2. Mathematical formulation

The bioconvection mixed convection hybrid nanofluid flow moving through a vertical surface in two-dimensional flow with adjusted magnetic field impacts is explored. Figure 1 exhibits the physical model with flow illustration where the uniform aligned magnetic field B_0 is applied and assumed to be variable kind with acute angle γ along the y-direction. When $\gamma = \pi/2$, this magnetic field behaves as a transverse magnetic field. The induced magnetic field is smaller than the applied magnetic field. Hence, the induced magnetic field is absent for a small magnetic Reynolds number. Suppose that the velocity distribution far from the plate is $u_e(x)$ while the temperature and concentration of the plate are denoted as $T_w(x)$ and $C_w(x)$, respectively. In addition, C_∞ and T_∞ are the concentration and the hybrid nanofluid temperature far from the plate, respectively.

Using these assumptions, the bioconvection hybrid nanofluid's boundary layer equations can be expressed as follows (Devi and Devi, 2017; Kuznetsov, 2010):

$$\frac{\partial u}{\partial x} + \frac{\partial v}{\partial y} = 0, \tag{1}$$

$$u\frac{\partial u}{\partial x} + v\frac{\partial u}{\partial y} = u_e\frac{du_e}{dx} + \frac{\mu_{hnf}}{\rho_{hnf}}\frac{\partial^2 u}{\partial y^2} - \frac{\sigma_{hnf}}{\rho_{hnf}}B_0^2\sin^2\gamma(u - u_e) + \frac{(\rho\beta)_{hnf}}{\rho_{hnf}}(T - T_\infty)g - \frac{\rho_\rho - \rho_{f_\infty}}{\rho_{hnf}}(C - C_\infty)g \tag{2}$$

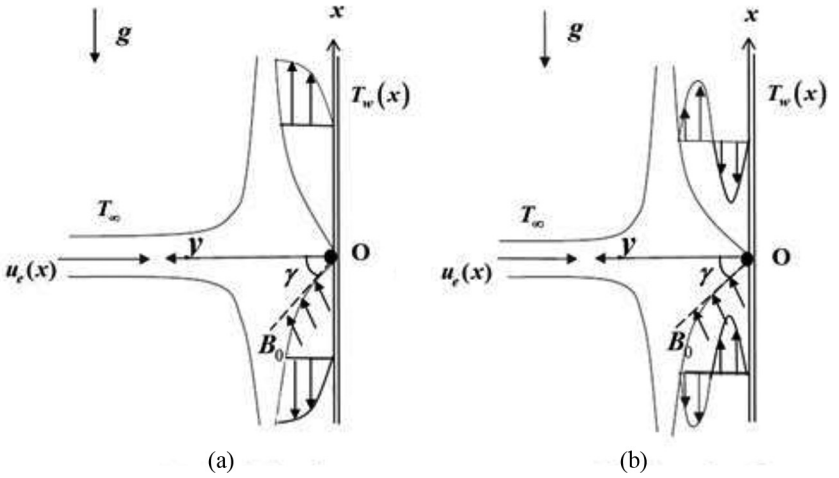

Figure 1.
Flow illustration: (a) assisting flow and (b) opposing flow

$$u\frac{\partial T}{\partial x}+v\frac{\partial T}{\partial y}=\frac{k_{hnf}}{(\rho C_p)_{hnf}}\frac{\partial^2 T}{\partial y^2}, \tag{3}$$

$$u\frac{\partial C}{\partial x}+v\frac{\partial C}{\partial y}=D_B\frac{\partial^2 C}{\partial y^2}, \tag{4}$$

$$u\frac{\partial N}{\partial x}+v\frac{\partial N}{\partial y}=D_n\frac{\partial^2 N}{\partial y^2}-\frac{bw_c}{\Delta C}\left[\frac{\partial}{\partial y}\left(N\frac{\partial C}{\partial y}\right)\right], \tag{5}$$

with

$$\begin{aligned} &u=0,\ v=0,\ T=T_w(x),\ C=C_w(x),\ N=N_w(x),\ \text{at } y=0,\\ &u\to u_e(x),\ T\to T_\infty,\ C\to C_\infty, N\to N_\infty,\quad \text{as } y\to\infty. \end{aligned} \tag{6}$$

From the given formulations, μ_{hnf} is the dynamic viscosity, ρ_{hnf} is the density, k_{hnf} is the thermal conductivity, $(\rho C_p)_{hnf}$ is the heat capacity of the hybrid nanofluid and σ_{hnf} is the electrical conductivity. Further, C_p is the heat capacity at the constant pressure, ρ is the density, while k is the thermal conductivity. Tables 1 and 2 display the correlation coefficient of the working fluid (Abu-Nada and Oztop, 2009; Devi and Devi, 2017; Takabi and Salehi, 2014).

Characteristics	Al_2O_3-Cu/H_2O
Thermal capacity	$(\rho C_p)_{hnf}=(1-\phi_{hnf})(\rho C_p)_f+\phi_1(\rho C_p)_{s1}+\phi_2(\rho C_p)_{s2}$
Dynamic viscosity	$\mu_{hnf}=\mu_f/(1-\phi_{hnf})^{2.5}$
Density	$\rho_{hnf}=(1-\phi_{hnf})\rho_f+\phi_1\rho_{s1}+\phi_2\rho_{s2}$
Electrical conductivity	$\frac{\sigma_{hnf}}{\sigma_f}=\left[\frac{\left(\frac{\phi_1\sigma_{s1}+\phi_2\sigma_{s2}}{\phi_{hnf}}\right)+2\sigma_f+2(\phi_1\sigma_{s1}+\phi_2\sigma_{s2})-2\phi_{hnf}\sigma_f}{\left(\frac{\phi_1\sigma_{s1}+\phi_2\sigma_{s2}}{\phi_{hnf}}\right)+2\sigma_f-(\phi_1\sigma_{s1}+\phi_2\sigma_{s2})+\phi_{hnf}\sigma_f}\right]$
Thermal conductivity	$\frac{k_{hnf}}{k_f}=\left[\frac{\left(\frac{\phi_1k_{s1}+\phi_2k_{s2}}{\phi_{hnf}}\right)+2k_f+2(\phi_1k_{s1}+\phi_2k_{s2})-2\phi_{hnf}k_f}{\left(\frac{\phi_1k_{s1}+\phi_2k_{s2}}{\phi_{hnf}}\right)+2k_f-(\phi_1k_{s1}+\phi_2k_{s2})+\phi_{hnf}k_f}\right]$

Table 1. Defined characteristics of Al_2O_3-Cu/H_2O (alumina-copper/water)

Physical properties	$\beta\times10^{-5}$(1/K)	k(W/mK)	C_p(J/kgK)	ρ(kg/m^3)
H_2O	21	0.613	4,179	997.1
Al_2O_3	0.85	40	765	3,970
Cu	1.67	400	385	8,933

Table 2. Base fluid and nanoparticles physical properties

Next, we take:

$$T_w(x) = T_\infty + T_0(x/L),\ C_w(x) = C_\infty + C_0(x/L),\\ N_w(x) = N_\infty + N_0(x/L),\ u_e(x) = ax, \tag{7}$$

where T_0 is the temperature characteristic of the plate surface with $T_0 < 0$ denotes the opposing flow and $T_0 > 0$ implies assisting flow; $C_0 > 0$ is the characteristic concentration of the plate; $N_0 > 0$ is the characteristic motile microorganism of the plate; and L is the characteristic length. Hereafter, a form-based similarity solution as follows (Kuznetsov, 2010; Avinash *et al.*, 2017) is considered:

$$u = axf'(\eta), v = -\sqrt{a\nu_f}f(\eta), \theta(\eta) = \frac{T - T_\infty}{\Delta T}, \phi(\eta) = \frac{C - C_\infty}{\Delta C},\\ \omega(\eta) = \frac{N - N_\infty}{\Delta N},\ \eta = y\sqrt{\frac{a}{\nu_f}}. \tag{8}$$

Here, the prime denotes differentiation concerning η, while $\Delta T = T_w - T_\infty$; $\Delta C = C_w - C_\infty$; and $\Delta N = N_w - N_\infty$. The following ordinary (similarity) differential equations are obtained by replacing equation (8) into equations (2)–(4):

$$\frac{\mu_{hnf}/\mu_f}{\rho_{hnf}/\rho_f}f''' + ff'' - f'^2 - \frac{\sigma_{hnf}/\sigma_f}{\rho_{hnf}/\rho_f}M(f' - 1)\sin^2\gamma + \left(\frac{\beta_{hnf}}{\beta_f}\theta - \Lambda\phi\right)\lambda + 1 = 0, \tag{9}$$

$$\frac{1}{\Pr}\frac{k_{hnf}/k_f}{(\rho C_p)_{hnf}/(\rho C_p)_f}\theta'' + f\theta' - f'\theta = 0, \tag{10}$$

$$\phi'' + Le\Pr(f\phi' - f'\phi) = 0, \tag{11}$$

$$\omega'' + Lb\Pr f\omega' - \mathrm{Pe}\left(\omega'\phi' + (\omega + \sigma)\phi''\right) = 0, \tag{12}$$

subject to the boundary conditions:

$$f(0) = 0, f'(0) = 0, \theta(0) = 1, \phi(0) = 1, \omega(0) = 1,\\ f'(\eta) \to 1, \theta(\eta) \to 0, \phi(\eta) \to 0, \omega(\eta) \to 0, \tag{13}$$

where Pr is the Prandtl number, Pe is the Peclet number and Le and Lb are the conventional Lewis number and the bioconvection Lewis number, respectively. Moreover, λ is the parameter of mixed convection, M and γ are the magnetic parameter and aligned angle, respectively, Λ is the buoyancy ratio parameter, while σ is a constant. The following are the definitions for the parameters mentioned above:

$$\Pr = (\rho C_p)_f/k_f,\ Le = \alpha_f/D_B,\ Lb = \alpha_f/D_n,\ \mathrm{Pe} = bw_c/D_n,\\ M = \sigma_f B_0^2/a\rho_f,\ \Lambda = (\rho_p - \rho_f)\Lambda C/\rho_f\beta_f\Delta T,\ \sigma = N_\infty/\Delta N,\ \lambda = g\beta_f T_0/a^2 L. \tag{14}$$

It should be pointed out that $\lambda > 0$ corresponds to assisting flow, $\lambda < 0$ corresponds to the opposing flow and $\lambda = 0$ describes the forced convection flow. We notice that equations (9) and (10) reduce to equations (17) and (18) from Ramachandran *et al.* (1988) when $\phi_1 = \phi_2 = 0$ and $M = \Lambda = 0$. The physical quantities of interest in the present work are expressed below:

$$C_f = \frac{\mu_{hnf}}{\rho_f u_e^2}\left(\frac{\partial u}{\partial y}\right)_{y=0}, Nu_x = -\frac{xk_{hnf}}{k_f \Delta T}\left(\frac{\partial T}{\partial y}\right)_{y=0}, Sh_x = -\frac{x}{\Delta C}\left(\frac{\partial C}{\partial y}\right)_{y=0},$$
$$Nn_x = -\frac{x}{\Delta N}\left(\frac{\partial N}{\partial y}\right)_{y=0}. \tag{15}$$

Using (8) and (15) we get:

$$\mathrm{Re}^{x1/2} C_f = \sqrt{\frac{m+1}{2}}\frac{\mu_{hnf}}{\mu_f} f''(0),\ \mathrm{Re}^{x-1/2} Nu_x = -\frac{k_{hnf}}{k_f}\theta'(0),$$
$$\mathrm{Re}^{x-1/2} Sh_x = -\phi'(0),\ \mathrm{Re}^{x-1/2} Nn_x = -\omega'(0),\ \text{where}\ \mathrm{Re}_x = u_e(x)x/\nu_f. \tag{16}$$

3. Analysis of solution stability

Since various solutions to the mathematical models (9)–(12) have been reported, the analysis of solution stability is examined. A special transformation variable, τ, is presented in the following way (Merrill *et al.*, 2006; Merkin, 1986):

$$u = ax\frac{\partial f}{\partial \eta}(\eta, \tau),\ v = -\sqrt{a\nu_f} f(\eta, \tau),\ \theta(\eta, \tau), = \frac{T - T_\infty}{T_w - T_\infty},$$
$$\phi(\eta, \tau), = \frac{C - C_\infty}{C_w - C_\infty},\ \omega(\eta, \tau), = \frac{N - N_\infty}{N_w - N_\infty},\ \eta = y\sqrt{\frac{a}{\nu_f}},\ \tau = at. \tag{17}$$

Employing (17) into equations (9)–(12), hence:

$$\frac{\mu_{hnf}/\mu_f}{\rho_{hnf}/\rho_f}\frac{\partial^3 f}{\partial \eta^3} + f\frac{\partial^2 f}{\partial \eta^2} - \left(\frac{\partial f}{\partial \eta}\right)^2 - \frac{\sigma_{hnf}/\sigma_f}{\rho_{hnf}/\rho_f} M\left(\frac{\partial f}{\partial \eta} - 1\right)\sin^2\gamma$$
$$+\left(\frac{\beta_{hnf}}{\beta_f}\theta - \Lambda\phi\right)\lambda - \frac{\partial^2 f}{\partial \eta \partial \tau} = 0, \tag{18}$$

$$\frac{1}{\mathrm{Pr}}\left(\frac{K_{hnf}/K_f}{(\rho C_p)_{hnf}/(\rho C_p)_f}\right)\frac{\partial^2 \theta}{\partial \eta^2} + f\frac{\partial \theta}{\partial \eta} - \frac{\partial f}{\partial \eta} - \frac{\partial \theta}{\partial \tau} = 0, \tag{19}$$

$$\frac{\partial^2 \phi}{\partial \eta^2} + Le\mathrm{Pr}\left(f\frac{\partial \theta}{\partial \eta} - \frac{\partial f}{\partial \eta}\phi\right) - \frac{\partial \theta}{\partial \tau} = 0, \tag{20}$$

$$\frac{\partial^2 \omega}{\partial \eta^2} + \mathrm{Pr}Lb\left(f\frac{\partial \omega}{\partial \eta}\right) - \mathrm{Pe}\left((\omega+\sigma)\frac{\partial^2 \phi}{\partial \eta^2} + \frac{\partial \omega}{\partial \eta}\frac{\partial \phi}{\partial \eta}\right) - \frac{\partial \omega}{\partial \tau} = 0, \tag{21}$$

with respect to:

$$\begin{aligned} &f(0,\tau) = 0, \frac{\partial f}{\partial \eta}(0,\tau) = 0, \theta(0,\tau) = 1, \phi(0,\tau) = 1, \omega(0,\tau) = 1, \\ &\frac{\partial f}{\partial \eta}(\eta,\tau) \to 1, \theta(\eta,\tau) \to 0, \phi(\eta,\tau) \to 0, \omega(\eta,\tau) \to 0. \end{aligned} \tag{22}$$

Next, the solutions of the steady flow can be studied where $f(\eta) = f_0(\eta)$, $\theta(\eta) = \theta_0(\eta)$, $\phi(\eta) = \phi_0(\eta)$ and $\omega(\eta) = \omega_0(\eta)$:

$$\begin{aligned} f(\eta,\tau) &= f_0(\eta) + e^{-\varepsilon\tau}F(\eta), \ \theta(\eta,\tau) = \theta_0(\eta) + e^{-\varepsilon\tau}G(\eta), \\ \phi(\eta,\tau) &= \phi_0(\eta) + e^{-\varepsilon\tau}H(\eta), \ \omega(\eta,\tau) = \omega_0(\eta) + e^{-\varepsilon\tau}I(\eta), \end{aligned} \tag{23}$$

is introduced based on the work of Weidman *et al.* (2006). Here, $F(\eta)$, $G(\eta)$, $H(\eta)$ and $I(\eta)$ are relatively small to $f_0(\eta)$, $\theta_0(\eta)$, $\phi_0(\eta)$ and $\omega_0(\eta)$ while ε is the unidentified eigenvalue. The eigenvalue problem (18)–(21) leading to an infinite number of eigenvalues $\varepsilon_1 < \varepsilon_2 < \varepsilon_{3\ldots}$ reflects a steady flow and an initial deterioration when ε_1 is positive. Meanwhile, when ε_1 is determined to be negative, therefore, an initial pattern of perturbations emerges. This discovery revealed the prevalence of unsteady flow. Replacing equation (23) into equations (18)–(21), hence:

$$\begin{aligned} \frac{\mu_{hnf}/\mu_f}{\rho_{hnf}/\rho_f}\frac{\partial^3 F}{\partial \eta^3} + f_0\frac{\partial^2 F}{\partial \eta^2} + F\frac{\partial^2 f_0}{\partial \eta^2} - 2\frac{\partial f_0}{\partial \eta}\frac{\partial F}{\partial \eta} - \frac{\sigma_{hnf}/\sigma_f}{\rho_{hnf}/\rho_f}M\left(\frac{\partial F}{\partial \eta} - 1\right)\sin^2\gamma \\ + \left(\frac{\beta_{hnf}}{\beta_f}G - \Lambda H\right)\lambda + \varepsilon\frac{\partial F}{\partial \eta} = 0, \end{aligned} \tag{24}$$

$$\frac{1}{\mathrm{Pr}}\left(\frac{K_{hnf}/K_f}{(\rho C_p)_{hnf}/(\rho C_p)_f}\right)\frac{\partial^2 G}{\partial \eta^2} + f_0\frac{\partial G}{\partial \eta} + F\frac{\partial \theta_0}{\partial \eta} - \theta_0\frac{\partial F}{\partial \eta} - G\frac{\partial f_0}{\partial \eta} + \varepsilon G = 0, \tag{25}$$

$$\frac{\partial^2 H}{\partial \eta^2} + Le\mathrm{Pr}\left(f_0\frac{\partial H}{\partial \eta} + F\frac{\partial \phi_0}{\partial \eta} - H\frac{\partial f_0}{\partial \eta} - \theta_0\frac{\partial F}{\partial \eta}\right) + \varepsilon H = 0, \tag{26}$$

$$\begin{aligned} \frac{\partial^2 I}{\partial \eta^2} + \mathrm{Pr}Lb\left(f_0\frac{\partial I}{\partial \eta} + F\frac{\partial \omega_0}{\partial \eta}\right) - Pe\left(\frac{\partial^2 \phi}{\partial \eta^2}I + \frac{\partial \phi_0}{\partial \eta}\frac{\partial I}{\partial \eta} + (\omega_0+\sigma)\frac{\partial^2 H}{\partial \eta^2} + \frac{\partial \omega_0}{\partial \eta}\frac{\partial H}{\partial \eta}\right) \\ + \varepsilon I = 0, \end{aligned} \tag{27}$$

$$\begin{aligned} &F(0) = 0, \frac{\partial F}{\partial \eta}(0) = 0, G(0) = 0, H(0) = 0, I(0) = 0, \\ &\frac{\partial F}{\partial \eta}(\eta) \to 0, G(\eta) \to 0, H(\eta) \to 0, I(\eta) \to 0, \end{aligned} \tag{28}$$

Now, we declare $f_0(\eta)$, $\theta_0(\eta)$, $\phi_0(\eta)$ and $\omega_0(\eta)$ as the steady-state flow's solutions which were executed by $\tau \to 0$. The linearized eigenvalue problem's solution is later discovered as:

$$\frac{\mu_{hnf}/\mu_f}{\rho_{hnf}/\rho_f}F''' + f_0F'' + Ff_0'' - 2f_0'F' - \frac{\sigma_{hnf}/\sigma_f}{\rho_{hnf}/\rho_f}M(F' - 1)\sin^2\gamma + \left(\frac{\beta_{hnf}}{\beta_f}G - \Lambda H\right)\lambda + \varepsilon F' = 0, \tag{29}$$

$$\frac{1}{\Pr}\left(\frac{K_{hnf}/K_f}{(\rho C_p)_{hnf}/(\rho C_p)_f}\right)G'' + f_0G' + F\theta_0' - \theta_0F' - Gf_0' + \varepsilon G = 0, \tag{30}$$

$$H'' + Le\Pr(f_0H' + F\phi_0' - Hf_0' - \theta_0F') + \varepsilon H = 0, \tag{31}$$

$$I'' + \Pr Lb(f_0I' + F\omega_0') - Pe(\phi_0'I' + \phi_0''I + (\omega_0 + \sigma)H'' + \omega_0'H') + \varepsilon I = 0, \tag{32}$$

$$\begin{aligned} &F(0) = 0, F'(0) = 0, G(0) = 0, H(0) = 0, I(0) = 0, \\ &F'(\eta) \to 0, G(\eta) \to 0, H(\eta) \to 0, I(\eta) \to 0, \quad \text{as} \quad \eta \to \infty. \end{aligned} \tag{33}$$

Further, by relaxing a boundary condition, the possible eigenvalues can be determined (Harris *et al.*, 2009). At this point, $F'(\eta) \to 0$ is set as $\eta \to \infty$, so the linearized eigenvalue problems (29)–(32) are exposed as $F''(0) \to 1$ when ε_1 is set up.

4. Results and discussion

The associated non-linear ordinary differential equations and subsequent boundary conditions are solved using the bvp4c method. Before achieving the desired outcome in bvp4c, the user is required to conduct multiple tries by offering an excellent preliminary prediction. The reliability of the numerical outputs is tested with Ramachandran *et al.* (1988) as accessible in Tables 3 and 4. The latest findings are strikingly comparable to previous research. Table 5 presents the values of $\mathrm{Re}_x^{1/2}C_f$, $\mathrm{Re}_x^{-1/2}Nu_x$, $\mathrm{Re}_x^{1/2}Sh_x$ and $\mathrm{Re}_x^{-1/2}Nn_x$ of Al_2O_3-Cu/H_2O for further references.

Table 3. $f''(0)$ and $-\theta'(0)$ with various Pr for assisting flow ($\lambda = 1.0$) while $\phi_1 = \phi_2 = \mathrm{Pe} = Le = Lb = M = \gamma = \Lambda = \beta = 0$

	$f''(0)$		$-\theta'(0)$	
Pr	Current result	Ramachandran *et al.* (1988)	Current result	Ramachandran *et al.* (1988)
0.7	1.706323	1.7063	0.764063	0.7641
7.0	1.517913	1.5179	1.722382	1.7224
20.0	1.448483	1.4485	2.457590	2.4576
40.0	1.410058	1.4101	3.101093	3.1011
60.0	1.390274	1.3903	3.551406	3.5514
80.0	1.377392	1.3774	3.909481	3.9095
100.0	1.368034	1.3680	4.211646	4.2116

The numerical calculations for different physical parameters used in the study were performed. A variety of values of ϕ_2 are implemented ($0.00 \leq \phi_2 \leq 0.01$), while ϕ_1 is fixed at 0.01. The nanoparticles assigned in this study are alumina (Al_2O_3) for ϕ_1 while copper (Cu) is denoted as ϕ_2. It must be highlighted that the values of the selected parameter should be used to generate an adequate preliminary estimation to obtain the desired result. Generally, ordinary differential equations, also referred to the similarity equations, produce non-unique solutions depending on the conditions. According to Merkin (1986), who introduced the perturbation method using an exponential function, the first solution is physically stable as the smallest eigenvalues are positive, which discloses a steady flow and initial deterioration. The second solution is stated unstable because the smallest eigenvalues are negative, exposing the unsteady flow and development of perturbations. Nevertheless, these findings are only applicable for dual solutions, and it is expected that different results will be obtained for a case study with more than two solutions (Weidman and Turner, 2017; Weidman, 2018).

In this study, beside a certain scale of a critical point, dual solutions are seen i.e. $\lambda_c < 0$. Conversely, when it regards to the occurrence of boundary layer separation, there is no solution found as $\lambda < \lambda_c$. Because there are two solutions in this study, a stability evaluation is necessary. The smallest eigenvalue ε_1 in the stability analysis technique denotes the dual solution's properties. Referring to Merkin (1986), the flow is defined stable when the smallest eigenvalues are more than 0. However, when the smallest eigenvalues are

Table 4. $f''(0)$ and $-\theta'(0)$ with different Pr for opposing flow ($\lambda = -1.0$) while $\phi_1 = \phi_2 = \text{Pe} = Le = Lb = M = \gamma = \Lambda = \beta = 0$

	$f''(0)$		$-\theta'(0)$	
Pr	Current result	Ramachandran *et al.* (1988)	Current result	Ramachandran *et al.* (1988)
0.7	0.691661	0.6917	0.633247	0.6332
7.0	0.923481	0.9235	1.546032	1.5403
20.0	1.003108	1.0031	2.268272	2.2683
40.0	1.045939	1.0459	2.905421	2.9054
60.0	1.067653	1.0677	3.352685	3.3527
80.0	1.081669	1.0817	3.708856	3.7089
100.0	1.091791	1.0918	4.009676	4.0097

Table 5. $\text{Re}_x^{1/2}C_f$, $\text{Re}_x^{-1/2}Nu_x$, $\text{Re}_x^{1/2}Sh_x$ and $\text{Re}_x^{-1/2}Nn_x$ when $\phi_1 = 0.01$, $M = 0.5$, $\lambda = -7.0$ and $\text{Pe} = 0.5$ for various values of ϕ_2, Le, Lb and γ

				Al_2O_3-Cu/water hybrid nanofluid ($\phi_1 = 0.01$)			
ϕ_2	γ	Le	Lb	$\text{Re}_x^{1/2}C_f$	$\text{Re}_x^{-1/2}Nu_x$	$\text{Re}_x^{1/2}Sh_x$	$\text{Re}_x^{-1/2}Nn_x$
0.00	$\pi/4$	0.50	0.50	0.353993	1.368511	1.067301	0.433071
0.005				0.345385	1.389631	1.067647	0.433818
0.01				0.336888	1.409697	1.067900	0.434513
0.01	$\pi/6$			0.267468	1.371092	1.042574	0.430262
	$\pi/4$			0.336888	1.409697	1.067900	0.434513
	$\pi/2$			0.507294	1.472740	1.109407	0.441667
	$\pi/4$	0.40		0.453965	1.463296	1.026619	0.476964
		0.50		0.336888	1.409697	1.067900	0.434513
		0.60		0.257051	1.362225	1.096926	0.400411
		0.50	0.50	–	–	–	0.434513
			0.60	–	–	–	0.491582
			0.70	–	–	–	0.541548

less than 0, the flow is considered inconsistent because it causes an early development of disturbances. As shown in the Table 6, the first solution is recognized as stable while the second solution is unreliable.

According to their findings, nanofluid stability reduces as volume concentration improves. Figures 2–5 define the effect of shifting the size of the nanoparticles $0.00 \leq \phi_2 \leq 0.01$ when ϕ_2 is varied. The increment in ϕ_2 reduces the behaviour of $f''(0)$ from Al_2O_3/H_2O to Al_2O_3-Cu/H_2O, as accessible in Figure 2. Meanwhile, the improvement in $-\theta'(0)$ corresponds to the rise of ϕ_2 is presented in Figure 3. The heating process was expedited by a greater value of nanoparticle volume ratio in Al_2O_3-Cu/H_2O compared to Al_2O_3/H_2O. In other sense, when the mass of the operating fluid upsurges, the surface temperature decreases, improving thermal performance and increasing the effectiveness of thermal conductivity in the opposing flow. Figure 4 describes the variability in the local Sherwood number $-\phi'(0)$ with several controlled parameters. The findings identified that with the increasing values of nanoparticles, $-\phi'(0)$ decreases. The same response is seen in Figure 5, which displayed the local motile microorganisms density number $-\omega'(0)$. When the opposing flow approaches the critical point λ_c, a decreasing trend of $-\omega'(0)$ is observed; however, the opposite behaviour is detected when the flow is distant from the critical point. Physically, this shows that a high concentration of nanoparticles generates huge resistance to the fluid motion, hence attributed to the decreasing values of $-\phi'(0)$ and $-\omega'(0)$.

Table 6.
Values of ε_1 with different λ

λ	First sol. ε_1	Second sol. ε_1
−9	0.2527	−0.2973
−9.3	0.1749	−0.2573
−9.53	0.1014	−0.2124
−9.637	0.0578	−0.1820
−9.7367	0.0015	−0.1379
−9.7387	0.00004	−0.1367

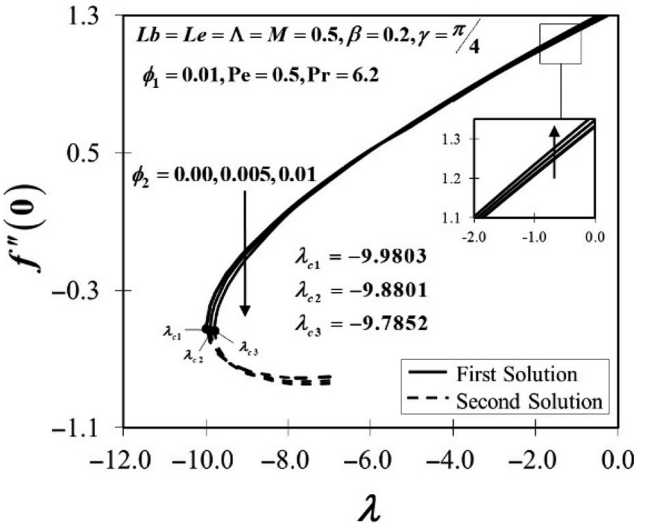

Figure 2.
$f''(0)$ towards λ varied by ϕ_2

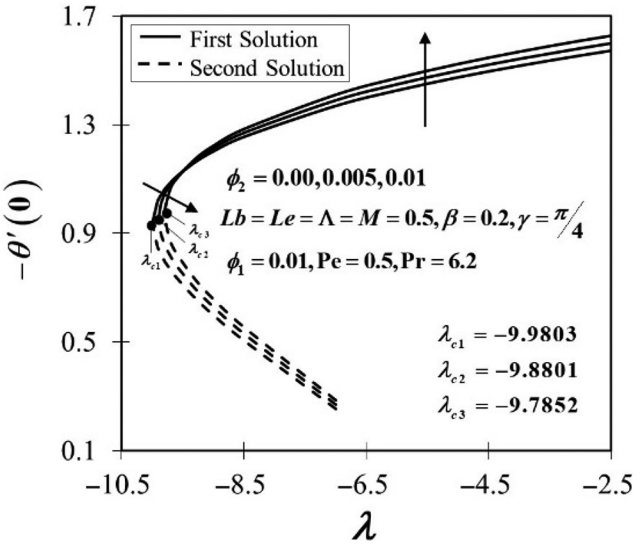

Figure 3.
$-\theta'(0)$ towards λ varied by ϕ_2

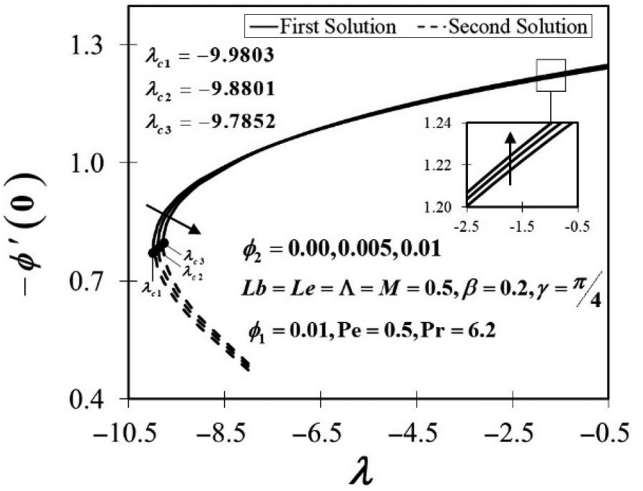

Figure 4.
$-\phi'(0)$ towards λ varied by ϕ_2

The Lorentz force in transport phenomena is well acknowledged to give a significant impact on fluid and heat transfer behaviour substantially. The Lorentz force, which is influenced substantially by the electromagnetic force, tends to slow down the fluid velocity and, consequently, raises the working fluid's temperature field. The findings in Figures 6–9 support this argument which is discussed in detail afterwards. The characteristic of $f''(0)$ for an elevation of aligned angle γ is illustrated in Figure 6. According to the findings, larger values of γ improve the trend of $f''(0)$ in Al_2O_3-Cu/H_2O. Due to the present of Lorentz drag effect, the nanofluid's velocity decreases as the aligned angle increases. The same pattern can be seen in the thermal properties $-\theta'(0)$ as γ exaggerated which is presented in Figure 7.

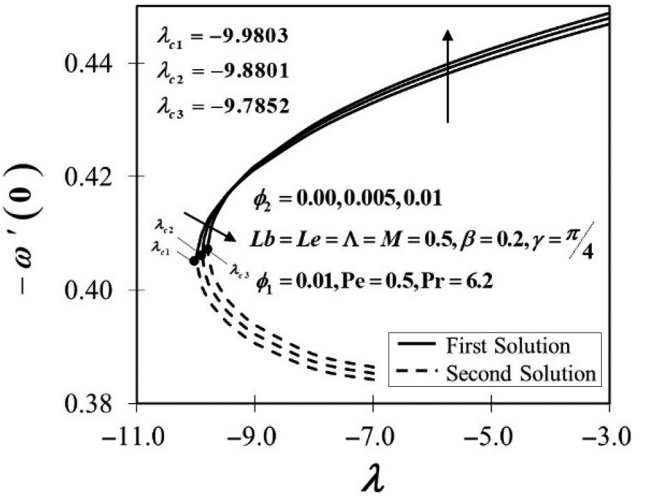

Figure 5.
$-\omega'(0)$ towards λ varied by ϕ_2

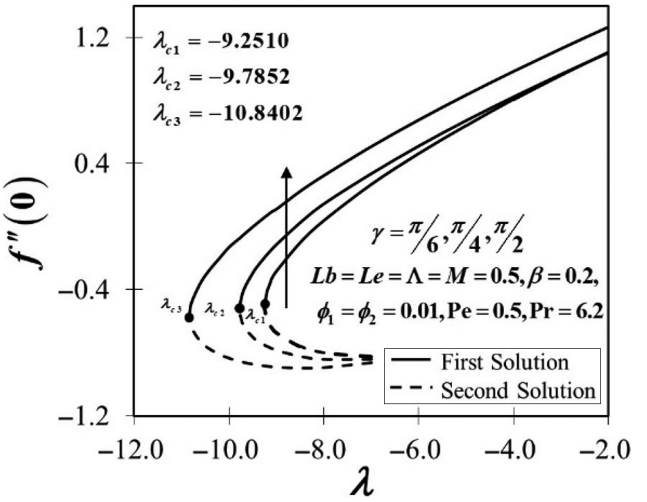

Figure 6.
$f''(0)$ towards λ varied by γ

Substantively, $-\theta'(0)$ lifts up once the aligned angle is added. The resistant Lorentz strength upsurges drag force past the shrinking plate, developing the fluid's temperature. Moreover, the transmission and development of the drag force into the flow helps to increase the temperature field, which ultimately increases the thickness of the thermal boundary layer. The influence of aligned angle parameter towards the microorganism concentration $-\phi'(0)$ and the motile microorganism density $-\omega'(0)$ are revealed in Figures 8 and 9. The finding indicates that behaviour of $-\phi'(0)$ and $-\omega'(0)$ on the Al_2O_3-Cu/H_2O flow is improved as γ rises for opposing flow. As previously stated, the aligned angle parameter increases fluid layer friction, resulting in increased thermal and concentration boundary layer thicknesses.

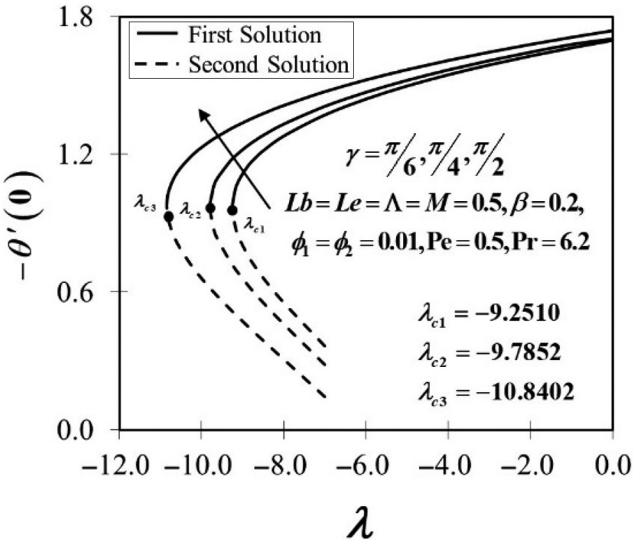

Figure 7.
$-\theta'(0)$ towards λ varied by γ

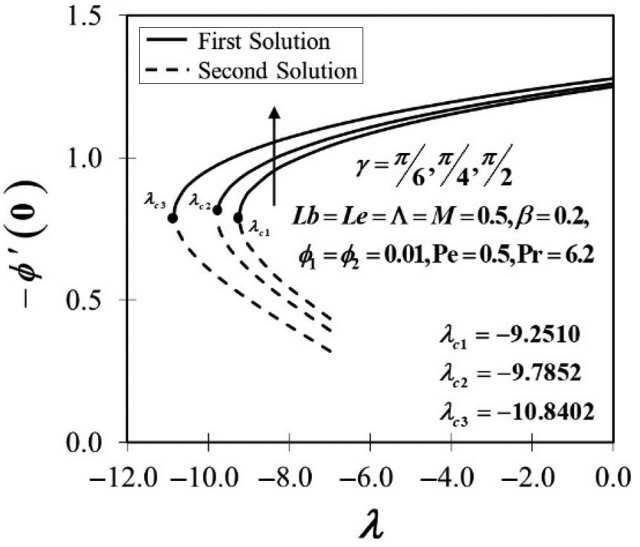

Figure 8.
$-\phi'(0)$ towards λ varied by γ

Figures 10–13 exhibit the impact of *Le* on the external force effects of the opposing flow. It is known that *Le* connects the thermal diffusivity to the concentration diffusivity of nanoparticles. The Al_2O_3-Cu/H_2O behaviour is depicted in Figure 10 concerning $f''(0)$ when the conventional Lewis number is varied where $Le = 0.4, 0.6, 0.7$ for opposing flow. Figure 10 depicts the addition of *Le* react to the decrement of $f''(0)$ (first solution), and vice versa for the second solution. The incline of *Le* results in thicker boundary layer which then lessens the velocity gradient, thus $f''(0)$ decreased. Due to the rise in the viscosity of Al_2O_3-Cu/H_2O,

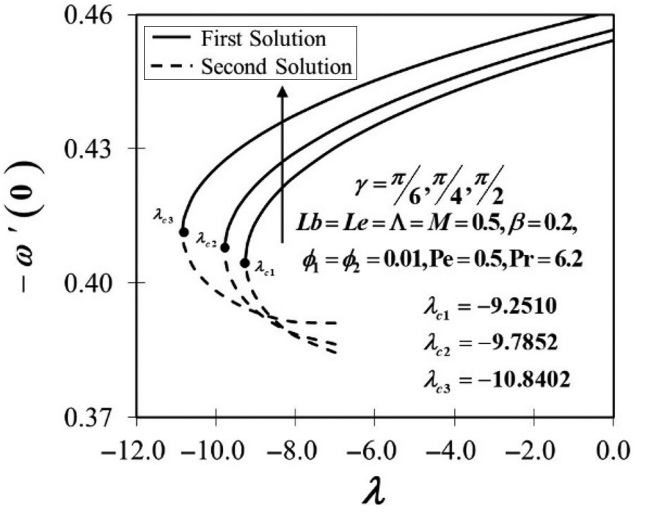

Figure 9.
$-\omega'(0)$ towards λ varied by γ

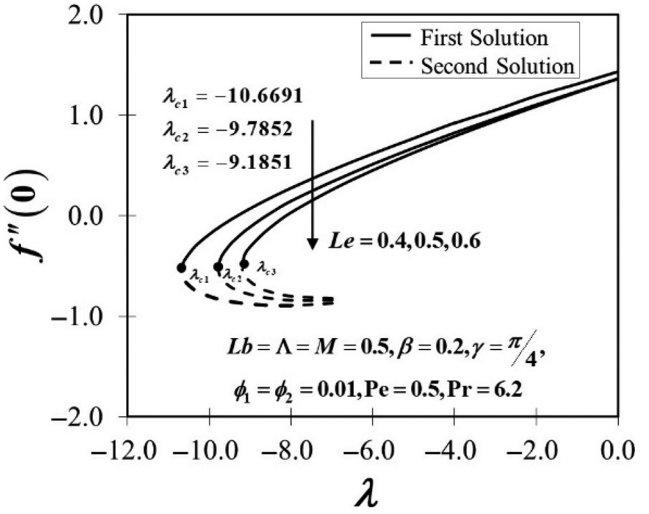

Figure 10.
$f''(0)$ towards λ varied by Le

the total concentration ($\phi_1 = \phi_2 = 0.01$) of nanoparticle volume fraction in the working fluid could also commence the diminution of $f''(0)$. Moreover, according to the following outcome in Figure 11, $-\theta'(0)$ is declined whilst Le grows the first solution. The conventional Lewis number parameter has a significant impact in heat transfer degradation. Figures 12 and 13 show a similar trend where the increment in Le exposed a downward trend of $-\phi'(0)$ and $-\omega'(0)$, in accordance with the conclusions by Acharya *et al.* (2016). Clearly, the influence of Le tends to lower the microorganism concentration and the motile microorganisms density.

The profile of velocity, temperature, concentration and density of the motile microorganisms is described in Figures 14–17 for opposing flow ($\lambda = -9.0$). When Le increased, $f'(\eta)$ shows an increase in the momentum boundary layer thickness of the first

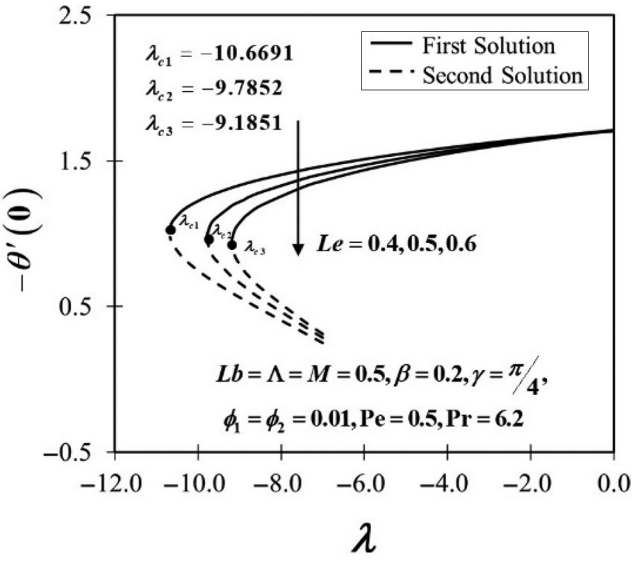

Figure 11.
$-\theta'(0)$ towards λ varied by Le

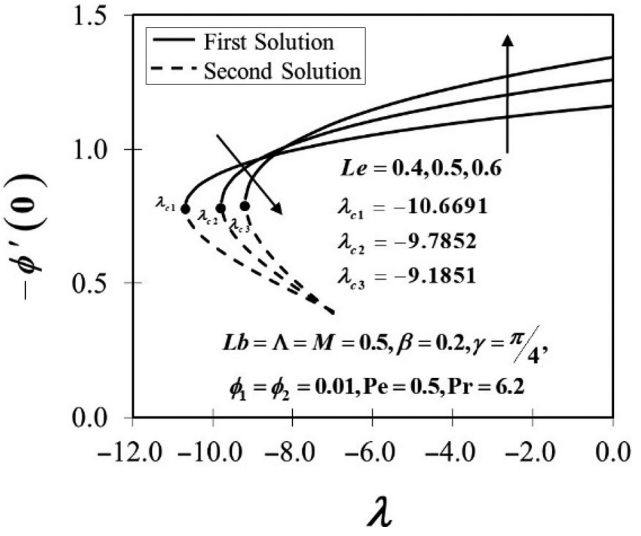

Figure 12.
$-\phi'(0)$ towards λ varied by Le

solution, as shown in Figure 14. However, the momentum boundary layer thickness in another solution decreases as the value of Le rises, as a result of which the velocity profile pattern is reverted. The temperature profile $\theta(\eta)$ with assorted Le is observed in Figure 15. Here, the Le parameter is discovered to be a cause of temperature rise, therefore improving the boundary layer thickness. An increase in Le causes a rise in temperature profiles, which degrades heat transfer performance and matches up to the result in Figure 11. Figure 16 demonstrates that the concentration profile $\phi(\eta)$ is depressed with increasing value of Le in

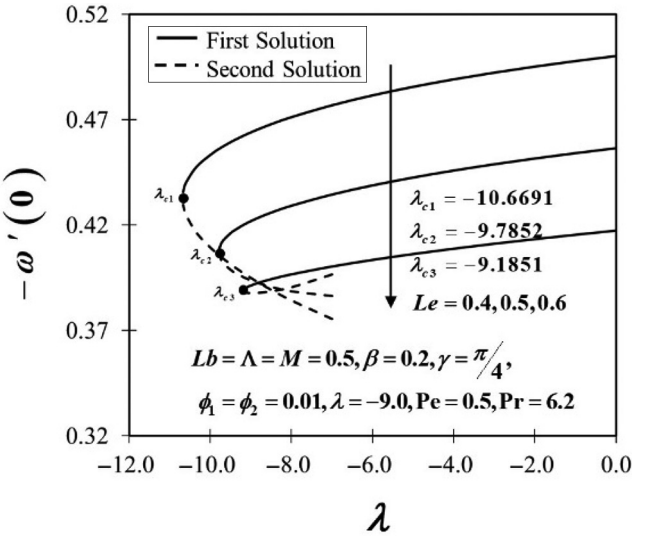

Figure 13.
$-\omega'(0)$ towards λ varied by *Le*

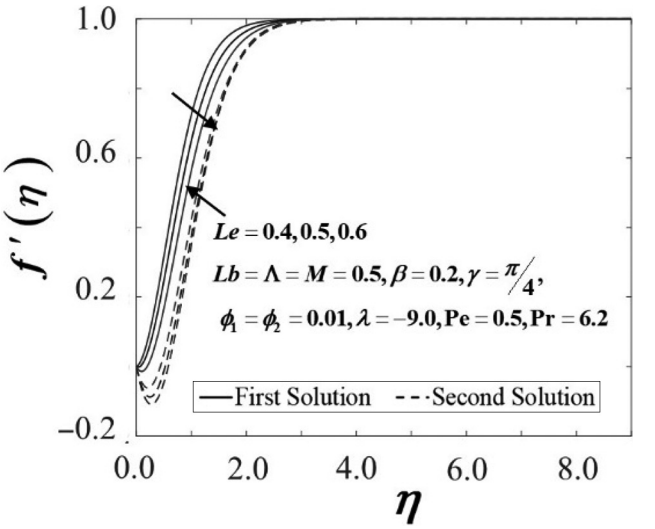

Figure 14.
$f'(\eta)$ with $\lambda = -9.0$ as *Le* differed

both solutions for opposing flow. The thickness of the boundary layer concentration declines as *Le* improves. Practically, the Lewis number reduces mass diffusivity, and reduces the penetration depth of the boundary layer concentration. The effects of *Le* on the motile microorganism density profile are revealed in Figure 17 where the profile shows an upward trend of the first solution, as *Le* increases. In contrast, the other solution depreciates dramatically as the Lewis number rises.

The response of the bioconvection Lewis parameter (*Lb*) towards the local density number of motile microorganisms $-\omega'(0)$ is displayed in Figure 18. It is clear to observe

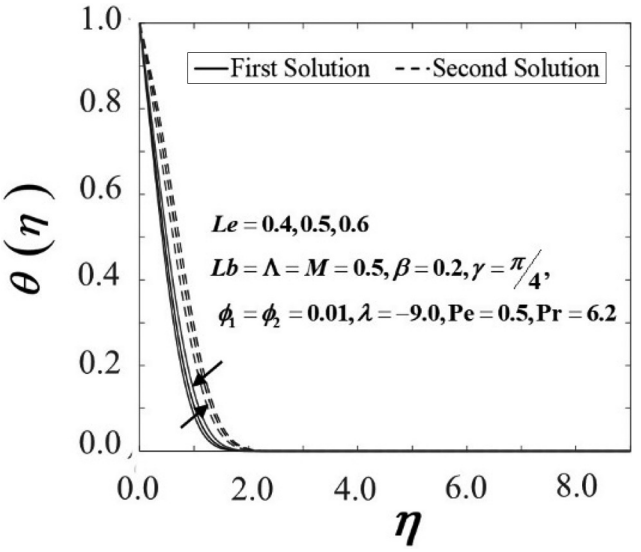

Figure 15.
$\theta(\eta)$ with $\lambda = -9.0$ as *Le* differed

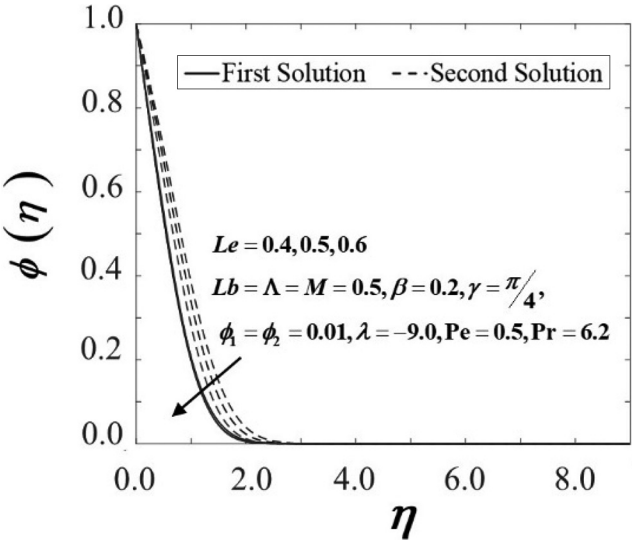

Figure 16.
$\phi(\eta)$ with $\lambda = -9.0$ as *Le* differed

that $-\omega'(0)$ is increased when *Lb* upsurges. As discussed in the previous results, the bioconvection Lewis number (*Lb*) is connected to the motile microorganisms' viscous diffusion rate (viscosity of nanofluid). The viscous diffusion rate increases as the bioconvection Lewis number rises, lowering the velocity at the surface, hence increased the $-\omega'(0)$. This may occur due to the fact that in the existence of bioconvection, the thermal diffusivity is much more prominent than the mass diffusivity, which diminishes molecule diffusivity as *Lb* increases, and this theoretically will enhance the heat transfer performance.

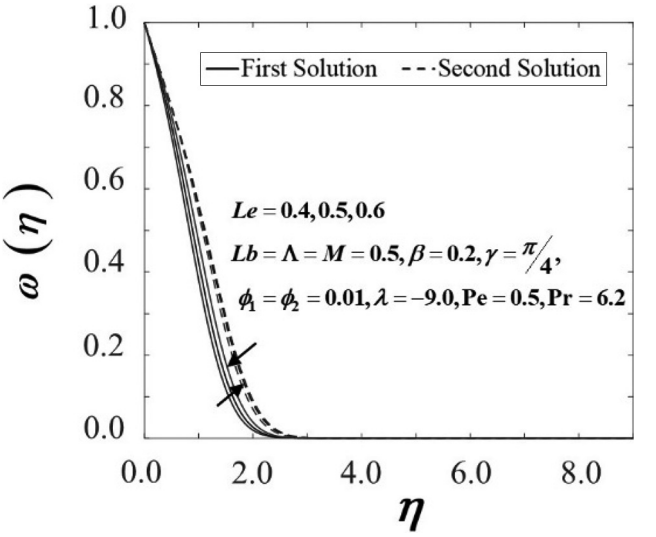

Figure 17.
$\omega(\eta)$ with $\lambda = -9.0$ as *Le* differed

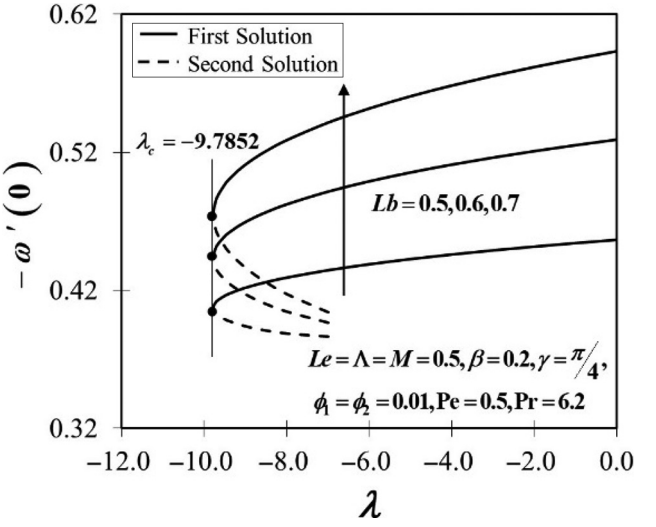

Figure 18.
$-\omega'(0)$ towards λ varied by *Lb*

In a nutshell, the concentration of nanoparticles, aligned angle, conventional Lewis number and bioconvection Lewis number have a significant impact on the system's properties of the current study.

5. Conclusions

In this study, a mathematical analysis on mixed bioconvection hybrid nanofluid flow towards a vertical plate including modified magnetic field effects and heat transfer was validated numerically. Several conclusions and future works are listed below:

- Dual solutions are conceivable throughout Al_2O_3-Cu/H_2O, which may be validated using certain controlling parameters.
- However, the dual solutions occur only at a certain range of the opposing flow. The first solution's consistency is guaranteed by the stability analysis, while the second solution is declared unstable.
- The inclusion of nanoparticle volume fraction diminished the skin friction coefficient, the local Sherwood number, and the local motile microorganism density number. On the other hand, the addition of nanoparticle volume fraction has been shown to increase the local Nusselt number in Al_2O_3-Cu/H_2O.
- However, when the number of nanoparticles and the aligned angle in the operating fluid rise, the thermal efficiency increases.
- The conventional Lewis number had subsequently been added, leading to an increase in the temperature profile. Thus, the thermal boundary layer is shifted upward, resulting in poor thermal conductivity.
- Additionally, the local density number of motile microorganisms in Al_2O_3-Cu/H_2O is declined attributed to the increasing values of conventional Lewis number.
- However, a different response towards the motile microorganism local density number is observed when the bioconvection Lewis number is enlarged.
- Further investigations are necessary to understand and investigate the heat transfer characteristics of this particular problem. For example, researchers can consider the unsteady flow of the mixed bioconvection stagnation point in hybrid nanofluid as this type of flow is not widely practiced. Additionally, the study of the bioconvective fields can be expended as well in the non-Newtonian hybrid nanofluid. The effect of slip boundary condition could also be incorporated, which plays an important role in the flow simulation and characteristics.

References

Abdul Hakeem, A.K., Indumathi, N., Ganga, B. and Nayak, M.K. (2020), "Comparison of disparate solid volume fraction ratios of hybrid nanofluids flow over a permeable flat surface with aligned magnetic field and Marangoni convection", *Scientia Iranica*, Vol. 27, pp. 3367-3380.

Abu-Nada, E. and Oztop, H.F. (2009), "Effects of inclination angle on natural convection in enclosures filled with Cu-water nanofluid", *International Journal of Heat and Fluid Flow*, Vol. 30 No. 4, pp. 669-678.

Acharya, N., Das, K. and Kundu, P.K. (2016), "Framing the effects of solar radiation on magneto-hydrodynamics bioconvection nanofluid flow in presence of gyrotactic microorganisms", *Journal of Molecular Liquids*, Vol. 222, pp. 28-37.

Al-Mdallal, Q.M., Indumathi, N., Ganga, B. and Abdul Hakeem, A.K. (2020), "Marangoni radiative effects of hybrid-nanofluids flow past a permeable surface with inclined magnetic field", *Case Studies in Thermal Engineering*, Vol. 17, p. 100571.

Anoop, K.B., Sundararajan, T. and Das, S.K. (2009), "Effect of particle size on the convective heat transfer in nanofluid in the developing region", *International Journal of Heat and Mass Transfer*, Vol. 52 Nos 9/10, pp. 2189-2195.

Anuar, N.S. and Bachok, N. (2021), "Double solutions and stability analysis of micropolar hybrid nanofluid with thermal radiation impact on unsteady stagnation point flow", *Mathematics*, Vol. 9, p. 276.

Arani, A.A.A. and Aberoumand, H. (2021), "Stagnation-point flow of Ag-CuO/water hybrid nanofluids over a permeable stretching/shrinking sheet with temporal stability analysis", *Powder Technology*, Vol. 380, pp. 152-163.

Ashwinkumar, G.P., Sulochana, C. and Samrat, S.P. (2018), "Effect of the aligned magnetic field on the boundary layer analysis of magnetic-nanofluid over a semi-infinite vertical plate with ferrous nanoparticles", *Multidiscipline Modeling in Materials and Structures*, Vol. 14 No. 3, pp. 497-515.

Avinash, K., Sandeep, N., Makinde, O.D. and Animasaun, I.L. (2017), "Aligned magnetic field effect on radiative bioconvection flow past a vertical plate with thermophoresis and Brownian motion", *Defect and Diffusion Forum*, Vol. 377, pp. 127-140.

Bees, M.A. and Croze, O.A. (2014), "Mathematics for streamlined biofuel production from unicellular algae", *Biofuels*, Vol. 5 No. 1, pp. 53-65.

Beg, O.A., Zohra, F.T., Uddin, M.J., Ismail, A.I.M. and Sathasivam, S. (2021), "Energy conservation of nanofluids from a biomagnetic needle in the presence of Stefan blowing: lie symmetry and numerical simulation", *Case Studies in Thermal Engineering*, Vol. 24, p. 100861.

Bhatti, M.M. and Michaelides, E.E. (2021), "Study of Arrhenius activation energy on the thermo-bioconvection nanofluid flow over a Riga plate", *Journal of Thermal Analysis and Calorimetry*, Vol. 143, pp. 2029-2038.

Choi, S.U. and Eastman, J. (1995), "Enhancing thermal conductivity of fluids with nanoparticles", *Proceedings of ASME International Mechanical Engineering Congress and Exposition*, Vol. 231, pp. 99-103.

Das, P.K. (2017), "A review based on the effect and mechanism of thermal conductivity of normal nanofluids and hybrid nanofluids", *Journal of Molecular Liquids*, Vol. 240, pp. 420-446.

Devi, S.U. and Devi, S.P.A. (2017), "Heat transfer enhancement of $Cu-Al_2O_3$/water hybrid nanofluid flow over a stretching sheet", *Journal of the Nigerian Mathematical Society*, Vol. 36, pp. 419-433.

Fisher, E.G. (1976), *Extrusion of Plastics*, Wiley, New York, NY.

Ghalambaz, M., Roşca, N.C., Roşca, A.V., Pop, I., Ros, N.C., Ros, A.V. and Pop, I. (2019), "Mixed convection and stability analysis of stagnation-point boundary layer flow and heat transfer of hybrid nanofluids over a vertical plate", *International Journal of Numerical Methods for Heat and Fluid Flow*, Vol. 30 No. 7, pp. 3737-3754.

Hamzah, M.H., Sidik, N.A.C., Ken, T.L., Mamat, R. and Najafi, G. (2017), "Factors affecting the performance of hybrid nanofluids: a comprehensive review", *International Journal of Heat and Mass Transfer*, Vol. 115, pp. 630-646.

Harris, S.D., Ingham, D.B. and Pop, I. (2009), "Mixed convection boundary-layer flow near the stagnation point on a vertical surface in a porous medium: Brinkman model with slip", *Transport in Porous Media*, Vol. 77 No. 2, pp. 267-285.

Hartmann, J. (1937), "Hg-DYNAMICS I", *Det Kongelige Danske Videnskabernes Selskab: Matematisk - Fysiske Meddelelser*, Vol. 15, pp. 1-28.

Hiemenz, K. (1911), "Die grenzschicht an einem in den gleichförmigen flüssigkeitsstrom eingetauchten geraden kreiszylinder", *Dingler's Polytechnisches Journal*, Vol. 326, p. 321.

Howarth, J.A. (1973), "A note on boundary-layer growth at an axisymmetric rear stagnation point", *Journal of Fluid Mechanics*, Vol. 59 No. 4, pp. 769-773.

Huminic, G. and Huminic, A. (2018), "Hybrid nanofluids for heat transfer applications – a state-of-the-art review", *International Journal of Heat and Mass Transfer*, Vol. 125, pp. 82-103.

Hussain, S., Jamal, M., Maatki, C., Ghachem, K. and Kolsi, L. (2021), "MHD mixed convection of Al_2O_3–Cu/water hybrid nanofluid in a wavy channel with incorporated fixed cylinder", *Journal of Thermal Analysis and Calorimetry*, Vol. 144 No. 6, pp. 2219-2233.

Jamaludin, A., Naganthran, K., Nazar, R. and Pop, I. (2020), "MHD mixed convection stagnation point flow of Cu-Al_2O_3/water hybrid nanofluid over a permeable stretching/shrinking surface with heat source/sink", *European Journal of Mechanics – B/Fluids*, Vol. 84, pp. 71-80.

Jamil, F. and Ali, H.M. (2020), *Applications of Hybrid Nanofluids in Different Fields*, Academic Press.

Janicek, A., Fan, Y. and Liu, H. (2014), "Design of microbial fuel cells for practical application: a review and analysis of scale-up studies", *Biofuels*, Vol. 5 No. 1, pp. 79-92.

Jo, J.H., Lee, D.S. and Park, J.M. (2006), "Modeling and optimization of photosynthetic hydrogen gas production by green alga *Chlamydomonas reinhardtii* in sulfur-deprived circumstance", *Biotechnology Progress*, Vol. 22 No. 2, pp. 431-437.

Katagiri, M. (1969), "On the separation of magnetohydrodynamic flow near the rear stagnation point", *Journal of the Physical Society of Japan*, Vol. 27 No. 4, pp. 1045-1050.

Khan, U., Waini, I., Ishak, A. and Pop, I. (2021), "Unsteady hybrid nanofluid flow over a radially permeable shrinking/stretching surface", *Journal of Molecular Liquids*, Vol. 331, p. 115752.

Khan, M.R., Li, M., Mao, S., Ali, R. and Khan, S. (2021), "Comparative study on heat transfer and friction drag in the flow of various hybrid nanofluids effected by aligned magnetic field and nonlinear radiation", *Scientific Reports*, Vol. 11, pp. 1-14.

Khashi'ie, N.S., Arifin, N.M., Merkin, J.H., Yahaya, R.I. and Pop, I. (2021), "Mixed convective stagnation point flow of a hybrid nanofluid toward a vertical cylinder", *International Journal of Numerical Methods for Heat and Fluid Flow*, Vol. 31 No. 12, doi: 10.1108/HFF-11-2020-0725.

Kuznetsov, A.V. (2010), "The onset of nanofluid bioconvection in a suspension containing both nanoparticles and gyrotactic microorganisms", *International Communications in Heat and Mass Transfer*, Vol. 37 No. 10, pp. 1421-1425.

Kuznetsov, A.V. and Avramenko, A.A. (2004), "Effect of small particles on this stability of bioconvection in a suspension of gyrotactic microorganisms in a layer of finite depth", *International Communications in Heat and Mass Transfer*, Vol. 31 No. 1, pp. 1-10.

Leibovich, S. (1967), "Magnetohydrodynamic flow at a rear stagnation point", *Journal of Fluid Mechanics*, Vol. 29 No. 2, pp. 401-413.

Merkin, J.H. (1986), "On dual solutions occurring in mixed convection in a porous medium", *Journal of Engineering Mathematics*, Vol. 20 No. 2, pp. 171-179.

Merrill, K., Beauchesne, M., Previte, J., Paullet, J. and Weidman, P. (2006), "Final steady flow near a stagnation point on a vertical surface in a porous medium", *International Journal of Heat and Mass Transfer*, Vol. 49 Nos 23/24, pp. 4681-4686.

Nadeem, S., Abbas, N. and Khan, A.U. (2018), "Characteristics of three dimensional stagnation point flow of hybrid nanofluid past a circular cylinder", *Results in Physics*, Vol. 8, pp. 829-835.

Pavlov, K.B. (1974), "Magnetohydrodynamic flow of an incompressible viscous fluid caused by deformation of a plane surface", *Magnitnaya Gidrodinamika*, Vol. 4, pp. 146-147.

Platt, J.R. (1961), "Bioconvection patterns in cultures of free-swimming organisms", *Science*, Vol. 133 No. 3466, p. 17661767.

Proudman, I. and Johsnon, K. (1961), "Boundary-layer growth near a rear stagnation point", *Journal of Fluid Mecanics.*, Vol. 12, pp. 161-168.

Raees, A., Xu, H., Sun, Q. and Pop, I. (2015), "Mixed convection in gravity-driven nano-liquid film containing both nanoparticles and gyrotactic microorganisms", *Applied Mathematics and Mechanics*, Vol. 36 No. 2, pp. 163-178.

Raju, C.S.K., Sandeep, N., Sulochana, C., Sugunamma, V. and Jayachandra Babu, M. (2015), "Radiation, inclined magnetic field and cross-diffusion effects on flow over a stretching surface", *Journal of the Nigerian Mathematical Society*, Vol. 34 No. 2, pp. 169-180.

Ramachandran, N., Chen, T.S. and Armaly, B.F. (1988), "Mixed convection in stagnation flows adjacent to vertical surfaces", *Journal of Heat Transfer*, Vol. 110 No. 2, pp. 373-377.

Rauwendaal, C. (1985), *Polymer Extrusion*, Hanser Publication, ed.

Robins, A.J. and Howarth, J.A. (1975), "Boundary-layerdevelopment at a two-dimensional rear stagnation point", *Journal of Fluid Mechanics*, Vol. 67, pp. 289-297.

Roşca, A.V., Roşca, N.C. and Pop, I. (2019), "Stagnation point flow of a nanofluid past a non-aligned stretching/shrinking sheet with a second-order slip velocity", *International Journal of Numerical Methods for Heat and Fluid Flow*, Vol. 29 No. 2, pp. 738-762.

Roşca, A.V., Roşca, N.C. and Pop, I. (2021d), "Mixed convection stagnation point flow of a hybrid nanofluid past a vertical flat plate with a second order velocity model", *International Journal of Numerical Methods for Heat and Fluid Flow*, Vol. 31 No. 1, pp. 75-91.

Roşca, N.C., Roşca, A.V. and Pop, I. (2021c), "Axisymmetric flow of hybrid nanofluid due to a permeable non-linearly stretching/shrinking sheet with radiation effect", *International Journal of Numerical Methods for Heat and Fluid Flow*, Vol. 31 No. 7, pp. 2330-2346.

Roşca, N.C., Roşca, A.V., Jafarimoghaddam, A. and Pop, I. (2021b), "Cross flow and heat transfer past a permeable stretching/shrinking sheet in a hybrid nanofluid", *International Journal of Numerical Methods for Heat and Fluid Flow*, Vol. 31 No. 4, pp. 1295-1319.

Rostami, M.N., Dinarvand, S. and Pop, I. (2018), "Dual solutions for mixed convective stagnation-point flow of an aqueous silica–alumina hybrid nanofluid", *Chinese Journal of Physics*, Vol. 56 No. 5, pp. 2465-2478.

Shah, T.R. and Ali, H.M. (2019), "Applications of hybrid nanofluids in solar energy, practical limitations and challenges: a critical review", *Solar Energy*, Vol. 183, pp. 173-203.

Sulochana, C., Sandeep, N., Sugunamma, V. and Rushi Kumar, B. (2016), "Aligned magnetic field and cross-diffusion effects of a nanofluid over an exponentially stretching surface in porous medium", *Applied Nanoscience*, Vol. 6 No. 5, pp. 737-746.

Takabi, B. and Salehi, S. (2014), "Augmentation of the heat transfer performance of a sinusoidal corrugated enclosure by employing hybrid nanofluid", *Advances in Mechanical Engineering*, Vol. 6, p. 147059.

Uddin, M.J., Bég, O.A. and Ismail, A.I. (2015), "Radiative convective nanofluid flow past a stretching/shrinking sheet with slip effects", *Journal of Thermophysics and Heat Transfer*, Vol. 29 No. 3, pp. 513-523.

Uddin, M.J., Kabir, M.N. and Bég, O.A. (2016), "Computational investigation of Stefan blowing and multiple-slip effects on buoyancy-driven bioconvection nanofluid flow with microorganisms", *International Journal of Heat and Mass Transfer*, Vol. 95, pp. 116-130.

Uddin, M.J., Kabir, M.N., Alginahi, Y. and Bég, O.A. (2000), "Numerical solution of bio-nano-convection transport from a horizontal plate with blowing and multiple slip effects", *Proceedings of the Institution of Mechanical Engineers, Part C: Journal of Mechanical Engineering Science*, Vol. 233, pp. 6910-6927.

Wager, H.W.T. (1911), "On the effect of gravity upon the movements and aggregation of *Euglena viridis*, *Ehrb*., and other micro-organisms", *Proceedings of the Royal Society of London. Series B, Containing Papers of a Biological Character*, Vol. 201, pp. 333-390.

Waini, I., Ishak, A. and Pop, I. (2020), "MHD flow and heat transfer of a hybrid nanofluid past a permeable stretching/shrinking wedge", *Applied Mathematics and Mechanics*, Vol. 41 No. 3, pp. 507-520.

Waini, I., Ishak, A. and Pop, I. (2021a), "Agrawal flow of a hybrid nanofluid over a shrinking disk", *Case Studies in Thermal Engineering*, Vol. 25, p. 100950.

Waini, I., Ishak, A. and Pop, I. (2021b), "Flow towards a stagnation region of a vertical plate in a hybrid nanofluid: assisting and opposing flows", *Mathematics*, Vol. 9 No. 4, pp. 1-16.

Weidman, P. (2018), "Hiemenz stagnation-point flow impinging on a biaxially stretching surface", *Meccanica*, Vol. 53 No. 4-5, pp. 833-840.

Weidman, P. and Turner, M.R. (2017), "Stagnation-point flows with stretching surfaces: a unified formulation and new results", *European Journal of Mechanics – B/Fluids*, Vol. 61, pp. 144-153.

Weidman, P.D., Kubitschek, D.G. and Davis, A.M.J. (2006), "The effect of transpiration on self-similar boundary layer flow over moving surfaces", *International Journal of Engineering Science*, Vol. 44 Nos 11/12, pp. 730-737.

Yang, L., Ji, W., Mao, M. and Huang, J.N. (2020), "An updated review on the properties, fabrication and application of hybrid-nanofluids along with their environmental effects", *Journal of Cleaner Production*, Vol. 257, p. 120408.

Zaimi, K., Ishak, A. and Pop, I. (2014), "Stagnation-point flow toward a stretching/shrinking sheet in a nanofluid containing both nanoparticles and gyrotactic microorganisms", *The Journal of Heat Transfer*, Vol. 136, pp. 1-10.

Zainal, N.A., Nazar, R., Naganthran, K. and Pop, I. (2020a), "MHD mixed convection stagnation point flow of a hybrid nanofluid past a vertical flat plate with convective boundary condition", *Chinese Journal of Physics*, Vol. 66, pp. 630-644.

Zainal, N.A., Nazar, R., Naganthran, K. and Pop, I. (2020b), "Unsteady stagnation point flow of hybrid nanofluid past a convectively heated stretching/shrinking sheet with velocity slip", *Mathematics*, Vol. 8 No. 10, p. 1649.

Zainal, N.A., Nazar, R., Naganthran, K. and Pop, I. (2021a), "Unsteady MHD mixed convection flow in hybrid nanofluid at three- dimensional stagnation point", *Mathematics*, Vol. 9 No. 5, p. 549.

Zainal, N.A., Nazar, R., Naganthran, K. and Pop, I. (2021b), "Unsteady EMHD stagnation point flow over a stretching/shrinking sheet in a hybrid Al_2O_3-Cu/H_2O nanofluid", *International Communications in Heat and Mass Transfer*, Vol. 123, p. 105205.

Zohra, F.T., Uddin, M.J. and Ismail, A.I. (2019), "Magnetohydrodynamic bio-nanoconvective naiver slip flow of micropolar fluid in a stretchable horizontal channel", *Heat Transfer-Asian Research*, Vol. 48 No. 8, pp. 3636-3656.

Zohra, F.T., Uddin, M.J., Basir, M.F. and Ismail, A.I.M. (2020), "Magnetohydrodynamic bio-nano-convective slip flow with Stefan blowing effects over a rotating disc", *Proceedings of the Institution of Mechanical Engineers, Part N: Journal of Nanomaterials, Nanoengineering and Nanosystems*, Vol. 234, pp. 83-97.

Further reading

Abdul Hakeem, A.K., Indumathi, N., Ganga, B. and Nayak, M.K. (2020), "Comparison of disparate solid volume fraction ratios of hybrid nanofluids flow over a permeable flat surface with aligned magnetic field and Marangoni convection", *Scientia Iranica*, pp. 3367-3380.

Anuar, N.S. and Bachok, N. (2021), "Double solutions and stability analysis of micropolar hybrid nanofluid with thermal radiation impact on unsteady stagnation point flow", *Mathematics*, Vol. 9 No. 3, p. 276.

Arani, A.A.A. and Aberoumand, H. (2021), "Stagnation-point flow of Ag-CuO/water hybrid nanofluids over a permeable stretching/shrinking sheet with temporal stability analysis", *Powder Technology*, Vol. 380, pp. 152-163.

Arifin, N.M., Nazar, R. and Pop, I. (2011), "Non-isobaric Marangoni boundary layer flow for Cu, Al_2O_3 and TiO_2 nanoparticles in a water-based fluid", *Meccanica*, Vol. 46 No. 4, pp. 833-843.

Bhatti, M.M. and Michaelides, E.E. (2021), "Study of Arrhenius activation energy on the thermo-bioconvection nanofluid flow over a Riga plate", *Journal of Thermal Analysis and Calorimetry*, Vol. 143 No. 3, pp. 2029-2038.

Huminic, G. and Huminic, A. (2018), "Hybrid nanofluids for heat transfer applications – a state-of-the-art review", *International Journal of Heat and Mass Transfer*, Vol. 125, pp. 82-103.

Proudman, I. and Johsnon, K. (1961), "Boundary-layer growth near a rear stagnation point", *Journal of Fluid Mechanics*, Vol. 12 No. 2, pp. 161-168.

Robins, A.J. and Howarth, J.A. (1975), "Boundary-layer development at a two-dimensional rear stagnation point", *Journal of Fluid Mechanics*, Vol. 67 No. 2, pp. 289-297.

Roşca, N.C. and Pop, I. (2021a), "Hybrid nanofluids flows determined by a permeable power-law stretching/shrinking sheet modulated by orthogonal surface shear", *Entropy*, Vol. 23 No. 7, p. 813.

Suresh, S., Venkitaraj, K.P. and Selvakumar, P. (2011), "Synthesis, characterisation of Al_2O_3-Cu nano composite powder and water based nanofluids", *Advanced Materials Research*, Vols 328/330, pp. 1560-1567.

Tiwari, R.K. and Das, M.K. (2007), "Heat transfer augmentation in a two-sided lid-driven differentially heated square cavity utilizing nanofluids", *International Journal of Heat and Mass Transfer*, Vol. 50 Nos 9/10, pp. 2002-2018.

Uddin, M.J., Kabir, M.N. and Bég, O.A. (2016), "Computational investigation of Stefan blowing and multiple-slip effects on buoyancy-driven bioconvection nanofluid flow with microorganisms", *International Journal of Heat and Mass Transfer*, Vol. 95, pp. 116-130.

Uddin, M.J., Sohail, A., Bég, O.A. and Ismail, A.M. (2018), "Numerical solution of MHD slip flow of a nanofluid past a radiating plate with Newtonian heating: A Lie group approach", *Alexandria Engineering Journal*, Vol. 57 No. 4, pp. 2455-2464.

Weidman, P. and Turner, M.R. (2017), "Stagnation-point flows with stretching surfaces: A unified formulation and new results", *European Journal of Mechanics – B/Fluids*, Vol. 61, pp. 144-153.

Corresponding author
Roslinda Nazar can be contacted at: rmn@ukm.edu.my